arXiv:1404.1924v2 [cond-mat.str-el] 20 Oct 2015

Emergent SU(3) symmetry in random spin-1 chains

V. L. Quito,[1] José A. Hoyos,[2] and E. Miranda[1]

[1] *Instituto de Física Gleb Wataghin, Unicamp, Rua Sérgio Buarque de Holanda, 777, CEP 13083-859 Campinas, SP, Brazil*
[2] *Instituto de Física de São Carlos, Universidade de São Paulo, C.P. 369, São Carlos, SP 13560-970, Brazil*

(Dated: October 22, 2015)

We show that generic SU(2)-invariant random spin-1 chains have phases with an emergent SU(3) symmetry. We map out the full zero-temperature phase diagram and identify two different phases: (i) a conventional random singlet phase (RSP) of strongly bound spin pairs (SU(3) "mesons") and (ii) an unconventional RSP of bound SU(3) "baryons", which are formed, in the great majority, by spin trios located at random positions. The emergent SU(3) symmetry dictates that susceptibilities and correlation functions of both dipolar and quadrupolar spin operators have the same asymptotic behavior.

PACS numbers: 75.10.Jm, 75.10.Pq, 75.10.Nr

Introduction.—Symmetries constitute a fundamental ingredient in our description of nature. In the standard model of elementary particles gauge symmetry is the organizing principle, strongly restricting the form of the microscopic equations [1]. In condensed matter systems, symmetries play a crucial role in classifying the various phases and transitions between them [2]. Symmetries can be destroyed at low energies, partially or completely, through the mechanism of spontaneous symmetry breaking. This is a familiar theme both in high-energy physics, as exemplified by the electroweak symmetry breaking, and at the condensed matter scale, in the various broken-symmetry phases of magnetism, superconductivity, superfluidity and others. The pattern of symmetry breaking, then, plays an important role in determining the spectrum of low-energy excitations (Goldstone bosons, quasiparticles, etc.) in the asymmetric phases [2].

A much less explored phenomenon is the enlargement of a system's symmetry at low energies. One of the earliest signs of such emergent symmetries was found in the critical region of the Ising chain in a transverse field, where the spectrum was predicted to be governed by the E_8 Lie group [3], which was later confirmed experimentally [4]. Other candidate systems have been proposed, both at fine-tuned critical points [5–7] and in extended phases [8–11]. Some proposals for quantum simulators of lattice gauge theories using cold atoms rely on the realization of the gauge symmetry as an emergent one [12].

Although a generic mechanism for the appearance of an emergent symmetry is not known, it has been suggested that such emergent symmetries arise when the ground state is a collection of subsystems coupled only by symmetry-breaking terms that are irrelevant in the renormalization-group (RG) sense [9, 13]. The emergent symmetry is, then, that of the subsystems.

In this Letter, we show that quenched disorder may also lead to an asymptotically decoupled ground state accompanied by an emergent global symmetry. We show that the most general disordered antiferromagnetic (AFM) SU(2)-symmetric spin-1 chain is characterized by an emergent SU(3) symmetry. At low energies, the system behaves as a collection of decoupled objects - namely: unbound SU(3) "quarks" and "antiquarks" plus bound SU(3) "mesons" or "baryons" - depending on the phase (see Fig. 1). As a consequence, susceptibilities and correlation functions of appropriately defined SU(3) operators (spin dipoles and quadrupoles) are governed by same universal exponents. Moreover, the emergent symmetry is identified in finite regions of parameter space and requires no fine tuning. As will become clear, this mechanism delineates a generic route towards emergent symmetries in strongly disordered systems.

The model.—We consider the most general SU(2)-symmetric random spin-1 chain given by the Hamiltonian

$$\mathcal{H} = \textstyle\sum_i \mathcal{H}_i = \displaystyle\sum_i \left[J_i \mathbf{S}_i \cdot \mathbf{S}_{i+1} + D_i \left(\mathbf{S}_i \cdot \mathbf{S}_{i+1} \right)^2 \right], \quad (1)$$

where J_i and D_i are independent random variables. In addition to condensed matter realizations, this may be especially relevant in cold-atom systems where spin couplings, dimensionality, and disorder can be controlled with considerable flexibility [14, 15].

The model is analyzed through the strong-disorder renormalization-group (SDRG) method [16–18] (for a general review see, e.g., Ref. [19] and for specific spin-1 systems, see [20–26]), which gives asymptotically exact results when the effective disorder grows without bound in the RG sense [27]. When this happens, the system is said to be governed by an infinite randomness fixed point (IRFP). As we will show, this is the case in the random singlet phases (RSPs) of our model (see Fig. 1).

It is useful to define the variable $\tan\theta_i = \frac{D_i}{J_i}$. The clean zero-temperature phase diagram has been extensively studied and shown to be quite rich (see, e.g., [28] and references therein). There is a conventional FM phase when $\frac{\pi}{2} < \theta < \frac{5\pi}{4}$. The system is gapped if $-\frac{3\pi}{4} < \theta < \frac{\pi}{4}$ and critical when $\frac{\pi}{4} < \theta < \frac{\pi}{2}$. For $-\frac{3\pi}{4} \leq \theta \leq -\frac{\pi}{4}$, the ground state is spontaneously dimerized. The topological Haldane phase extends from $-\frac{\pi}{4}$ to $\frac{\pi}{4}$. Moreover, some

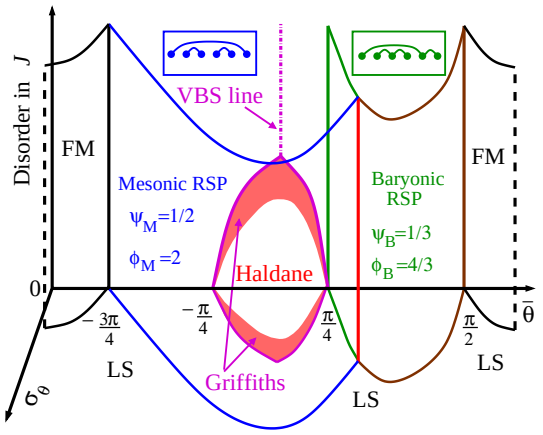

Figure 1. Phase diagram of the random spin-1 chain. The angle θ is defined through the ratio between biquadratic and bilinear couplings $\tan\theta_i = \frac{D_i}{J_i}$. Solid lines represent continuous transitions. The Haldane phase is characterized by a finite gap and topological order. In the red (shaded) Griffiths region the gap vanishes but the topological order remains. At stronger disorder, there is a conventional "mesonic" RSP and an unconventional "baryonic" RSP. In the latter, the singlets are formed mostly out of spin trios. The insets depict schematically the corresponding random-singlet ground states. LS and FM stand for Large Spin and ferromagnetic phases, respectively.

special points are noteworthy: the Affleck-Kennedy-Lieb-Tasaki (AKLT) point ($\tan\theta = \frac{1}{3}$, with $J > 0$), at which the ground state is known to be a valence bond solid (VBS), four SU(3)-symmetric points $\theta = \frac{\pi}{4}$, $\theta = \pm\frac{\pi}{2}$ and $\theta = -\frac{3\pi}{4}$, and the critical point $\theta = -\frac{\pi}{4}$.

The decimation procedure.—We now describe the SDRG decimation procedure assuming strong disorder (the weak-disorder regime is discussed in the Supplemental Material [29]). The idea is to obtain a description of the low-energy sector by gradually eliminating high-energy excitations of small clusters and finding the effective Hamiltonian of the remaining degrees of freedom. We define the ith gap Δ_i as the energy difference between the ground and the first excited state of the local Hamiltonian $\mathcal{H}_i$. At each step, we look for the largest gap say, $\Delta_2 = \max(\Delta_i) \equiv \Omega$, keep only the lowest-energy multiplet of $\mathcal{H}_2$, and use perturbation theory to find how the remaining degrees of freedom are coupled.

The possible steps are depicted in Fig. 2(a). When the ground state of $\mathcal{H}_2$ is a singlet ($-\frac{3\pi}{4} < \theta_2 < \arctan\frac{1}{3}$), spins S_2 and S_3 are removed and the new effective couplings between spins S_1 and S_4 are

$$\tilde{K} = \frac{4K_1K_3}{3\left(K_2 - \frac{5}{2}D_2\right)}, \quad \tilde{D} = -\frac{2D_1D_3}{9\left(K_2 - \frac{1}{2}D_2\right)}, \qquad (2)$$

where $K_i = J_i - D_i/2$ [36]. On the other hand, when the ground state is a triplet ($\arctan\frac{1}{3} < \theta_2 < \frac{\pi}{2}$), the pair is replaced by a new spin 1 degree of freedom coupled to S_1 and S_4 via

$$\tilde{K}_i = \frac{1}{2}K_i, \quad \tilde{D}_i = -\frac{1}{2}D_i, \qquad (3)$$

with $i = 1, 3$. Finally, when $\frac{\pi}{2} < \theta_2 < \frac{5\pi}{4}$, the ground state is a quintuplet, the spin pair can be replaced by an effective spin-2 degree of freedom and the new effective couplings are $\tilde{K}_i = \frac{1}{2}K_i$ and $\tilde{D}_i = \frac{1}{24}D_i$. It turns out that the renormalized Hamiltonian retains the form (1), albeit with different spins and new couplings, as previously reported in [37].

SDRG flows.—Inspection of Eqs. (2) and (3) allows us to immediately identify four fixed points (FPs) of the SDRG flow. They are characterized by fixed angles θ_i. We denote them by numbers [see solid red stars in Fig. 2(a)], as follows.

(1) The FP $D_i = 0$, with $K_i = J_i > 0$ ($\theta_i = 0$), is the disordered AFM Heisenberg chain, which was intensively studied in Refs. [20–24]. For strong enough disorder, the flow is towards an IRFP (the relative width of the distribution of couplings grows without bounds) and the ground state is a collection of nearly independent singlets formed between arbitrarily distant spin pairs - a conventional random singlet (RS) state.

(2) The FP $K_i = 0$ with $D_i < 0$ ($\theta_i = \arctan 2$ in the third quadrant), which corresponds to a flow similar to FP (1) since all decimations are of singlet-formation type [see Fig. 2(a)] and lead to the same conventional RS state.

(3) The FP $K_i = 0$ with positive and negative D_i ($\theta_i = \arctan 2$, with θ_i in both the first and third quadrants). This FP involves SDRG steps of both singlet- and triplet-generating types [see Fig. 2(a)]. Here, the effective system has equal fractions of positive and negative $\tilde{D}_i$'s (and, hence, equal fractions of singlet- and triplet-generating decimations), since this is the only situation that is preserved by the RG flow. Although this

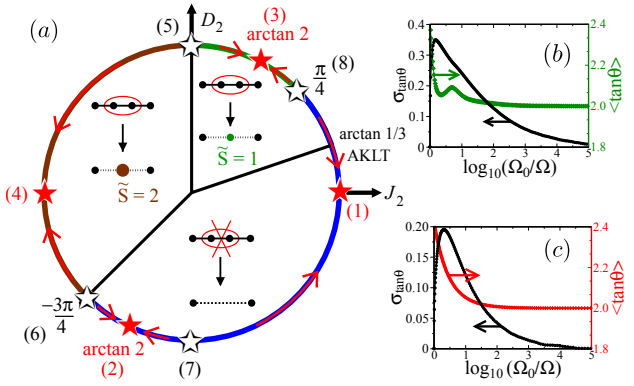

Figure 2. (a) SDRG decimation steps, fixed points and basins of attraction. Solid (open) stars denote stable (unstable) fixed points. (b) and (c) show the average and width of the $\tan\theta_i$ distribution along the SDRG flow. Initially, (b) $\theta_i = 3\pi/8$ and (c) $\theta_i = -5\pi/8$, with $\sigma_{\tan\theta} = 0$ in both cases.

FP actually encompasses both signs of D_i, we choose to represent it by a single star in the first quadrant. The presence of both types of decimations leads to a state different from FPs (1) and (2) above. In fact, this SDRG flow is, up to irrelevant numerical prefactors, identical to that of generic SU(3)-symmetric chains discussed in [38]. We will come back to this point later.

(4) The FP $D_i = 0$, with $K_i = J_i < 0$ ($\theta_i = \pi$), which corresponds to the disordered FM Heisenberg chain. As spins larger than 2 are generated in this case, the decimation procedure must be complemented by those of ref. [39]. This FM state is not the focus of this Letter and will be considered elsewhere [40].

It is straightforward to show [29] that the FPs (1)-(3) are stable with respect to narrow distributions of angles θ_i. Moreover, our extensive numerics indeed confirm that these are the only four stable FPs. Thus, there must be four other unstable ones [depicted as open stars in Fig. 2(a)]. The strongest candidates are the four SU(3)-symmetric points $\theta_i = \pm\frac{\pi}{2}, \frac{\pi}{4}$, and $-\frac{3\pi}{4}$, since this global symmetry is preserved by the SDRG. Although our methods cannot be used precisely *at* the FM points $\theta_i = \frac{\pi}{2}$ and $\theta_i = -\frac{3\pi}{4}$, we have checked numerically that the SDRG flow is always away from them [29]. We thus conjecture they are unstable FM FPs and denote them by (5) and (6), respectively.

We now show that the other two, $\theta_i = \frac{\pi}{4}$ and $\theta_i = -\frac{\pi}{2}$, are indeed FPs. As it will be important for the understanding of the emergent SU(3) symmetry, we will describe these points in detail. The Hamiltonian at these points can be recast as [29]

$$H = \sum_i \sum_{a=1}^{8} C_i \Lambda_{a,i} \cdot \Lambda_{a,i+1} + \text{const} \qquad (4)$$

where $\Lambda_{a,i}$ ($a = 1, \ldots, 8$) are the generators of an irreducible representation (IR) of SU(3). When $\theta_i = -\frac{\pi}{2}$, $C_i = |D_i|/2$ and the IR on odd (even) sites is the fundamental (antifundamental) one, also called the quark (antiquark) IR. As can be verified from Eq. (2), this FP is characterized by singlet formation only. At each step a quark binds to an antiquark to form a singlet (a meson, in QCD language). Note that the alternation of quarks and antiquarks in the chain is preserved by this flow. It thus realizes the same kind of RS state of the FPs (1) and (2) above. We will, accordingly, dub it a mesonic RS state and number it as (7).

When $\theta_i = \frac{\pi}{4}$, the IR is the quark one on every site and $C_i = J_i/2$. Decimation of a bond with $\frac{\pi}{4}$ turns the adjacent bond angles into $-\frac{\pi}{2}$ [see Eq. (3)]. There is, thus, a quick proliferation of bonds with $\theta_i = -\frac{\pi}{2}$. Further decimation of a bond with $\theta_i = -\frac{\pi}{2}$ leads to a spin singlet and an effective bond angle of $-\frac{\pi}{2}$, if $\theta_{i-1} = \theta_{i+1}$, or $\frac{\pi}{4}$ otherwise [see Eqs. (2) and (3)]. The SDRG flow for this FP, which we will number as (8), is characterized by equal fractions of bonds with $\theta_i = \frac{\pi}{4}$ and $\theta_i = -\frac{\pi}{2}$ (again, this is the only situation preserved by the flow [29]). In SU(3) language, two original quarks first bind to form an effective antiquark [38] [the effective spin 1 of the decimation step of Eq. (3)]. This antiquark can later bind to a third quark to form a singlet. Effectively, this singlet is formed out of three original quarks, just like a baryon is formed out of three valence quarks [41]. Note that the structure of this SDRG flow is the same as that of FP (3), even though the couplings and angles are not the same. We call this a baryonic RS state. For simplicity, as in case (3), this case (8) is represented somewhat imprecisely by a single star in the first quadrant.

Phase diagram.—The identification of all FPs and their stability properties allow for the immediate description of three basins of attraction for initial strongly disordered distributions of coupling constants with a fixed angle $\theta_i = \theta_0$ for all i (the initial angle distribution width $\sigma_\theta = 0$), as shown by the differently colored arcs along the circumference of Fig. 2(a). The red arrows show the flow direction, with the caveat that the flow towards the FP (3) (the green arc) also involves excursions into region $-\frac{3\pi}{4} < \theta \leq -\frac{\pi}{2}$. We have verified numerically that these are indeed the only possible flows [29]. Two typical examples are shown in Figs. 2(b) and (c). Note that the distribution widths initially grow but eventually vanish as the stable FPs are approached. This is to be expected, since the stable FPs are characterized by a unique value of $\tan\theta$. In other words, $\sigma_{\tan\theta}$ is an irrelevant variable at the stable FPs. As discussed in greater detail in the Supplemental Material [29], we only expect the behavior found in the strong-disorder regime to break down inside a dome around the Haldane phase $-\frac{\pi}{4} < \theta_0 < \frac{\pi}{4}$. This allows us to obtain the phase diagram shown in Fig. 1 on the plane $\sigma_\theta = 0$.

We now describe the physical properties of the various phases. In the whole region $-\frac{3\pi}{4} < \theta_0 < \frac{\pi}{4}$ [the blue arc of Fig. 2(a)], all decimations lead, after an initial transient, to the formation of ever-more-widely separated singlet pairs (no trios) and the ground state is analogous to the RSP of the spin-1/2 AFM Heisenberg chain [27]. The flow is attracted by either of the two stable FPs (1) and (2). Since their structure is the same as the unstable SU(3)-symmetric FP (7), we describe this whole region as a mesonic RSP. The properties of such phases are well known [27]. The energy (Ω) and length (L) scales of excitations obey activated dynamical scaling $\ln\Omega \sim -L^\psi$ with a universal $\psi = \psi_M = \frac{1}{2}$, the magnetic susceptibility diverges as $\chi \sim 1/\left(T\,|\ln T|^{1/\psi}\right)$, and the specific heat vanishes as $c \sim |\ln T|^{-(1+1/\psi)}$ as $T \to 0$. The typical ground-state spin-spin correlations vanish as $\sim \exp\left(-\text{const} \times |i-j|^\psi\right)$, as a consequence of the localized nature of the phase, whereas the average correlations are dominated by the spin singlets and vanish only algebraically $\sim e^{iq(i-j)}\,|i-j|^{-\phi}$, with $q = q_M = \pi$ and a

universal exponent $\phi = \phi_M = 2$. The difference between the two FPs lies in the nature of the excitations. For $-\frac{\pi}{2} < \theta_0 < \frac{\pi}{4}$, the lowest excitation of a random singlet pair has spin 1, whereas for $-\frac{3\pi}{4} < \theta_0 < -\frac{\pi}{2}$, it has spin 2. At the SU(3)-symmetric FP (7), the two types of excitations become degenerate and are analogous to the meson octuplets of QCD.

In the region $\frac{\pi}{4} < \theta_0 < \frac{\pi}{2}$ [the green arc of Fig. 2(a)] the flow converges to the FP (3) and is characterized by the formation of baryonic-like singlet trios (and also rarer sextets, etc.). In fact, the same happens for $\theta_0 = \frac{\pi}{4}$ [the unstable SU(3)-symmetric one FP (8)]. As a result, as shown in [38], the low-energy physical properties of this baryonic RSP have the same generic forms as in the mesonic RSP, but with $q = q_B = 2\pi/3$ and the important difference that the universal exponents change to $\psi = \psi_B = 1/3$ and $\phi = \phi_B = 4/3$.

We now address the case when the initial distribution of angles has a nonzero width σ_θ. We have verified numerically that the phase diagram is still valid as long as *all* the initial angles lie inside the basin of attraction of the corresponding phase. Otherwise, the flow is more involved. When the mesonic and the baryonic RSPs initially compete, the former absorbs the flow. When the FM phase competes with any of the others, the system flows to the so-called Large Spin phase [39], as a consequence of the presence of both AFM and FM couplings. With this, we complete the topology of the phase diagram of Fig. 1.

Emergent SU(3) symmetry.—A few elements of the flow to an IRFP completely determine the low- and zero-temperature properties of the system. In the present case, these elements are (i) a ground state made up of strongly coupled singlet-forming spins, pairs in the case of FPs (1), (2), and (7), and (mostly) trios at FPs (3) and (8), with well-characterized size distributions [27, 38, 42], and (ii) low-energy excitations consisting of essentially free spin-1 clusters with known scale-dependent density [18, 27, 38]. We now show that both elements have SU(3) symmetry and this gives rise to an emergent SU(3) symmetry in extended regions of the phase diagram. Indeed, the singlets of element (i) are not only SU(2) but also SU(3) singlets. In addition, the spin-1 clusters of element (ii) transform as SU(3) quarks or antiquarks. This can be more easily seen from the fact that the ground multiplets of the singlet- and triplet-generating decimation steps of Eqs. (2) and (3) are all θ-independent. In other words, the ground states at the FPs (1), (2) and (7) are the same, and so are the ground states of FPs (3) and (8). This leads immediately to the result that, at $T = 0$, the average and typical correlation functions of all SU(3) generators Λ_a ($a = 1, \ldots 8$), which include dipolar and quadrupolar spin operators, are governed by the same exponents (ψ_H, ϕ_H) with $H = M$ or B. For a complete list of these operators, see the Supplemental Material [29].

Likewise, the low-temperature SU(3) susceptibilities of the RSPs can be written as [18, 38]

$$\chi_a(T) \approx n(\Omega = T)\, \chi_a^{\text{free}}(T), \tag{5}$$

where $n(\Omega) = \frac{N(\Omega)}{L_0}$ is the density of undecimated spin clusters at the scale Ω and $\chi_a^{\text{free}}(T)$ is the SU(3) susceptibility of a free spin cluster. Since the free spin clusters (triplets) are SU(3) quarks or antiquarks, $\chi_a^{\text{free}}(T)$ is SU(3) symmetric and independent of a. Taking, e.g., $\Lambda_3 = \tilde{\Lambda}_3 = S_z$, $\chi_a^{\text{free}}(T) = 2/(3T)$ for both representations. Since $n(\Omega = T) \sim 1/|\ln T|^{1/\psi_H}$ [29], we get $\chi_a \sim 1/\left(T\,|\ln T|^{1/\psi_H}\right)$.

The emergent symmetry occurs even at the Heisenberg point (1), a feature previously unnoticed. We stress that although these various quantities are all governed by the same exponents, the numerical prefactors are *not* the same due to the initial inexactness of the SDRG procedure. A similar phenomenon is observed in disordered spin-$\frac{1}{2}$ XXZ chains, in which, despite the absence of global SU(2) symmetry, both longitudinal and transverse correlations and susceptibilities are governed by the same exponents [27].

Conclusions.— We have found the generic route towards emergent symmetries at IRFPs: the ground multiplets of the two-spin problem (of the SDRG) must transform as irreducible representations of the emergent symmetry. In the present case, the singlet and the triplet states are SU(3) symmetric. The simplicity of the mechanism responsible for the emergent symmetry that we uncovered suggests that it might find other realizations. We have looked for them in generic disordered SU(2)-invariant spin-S chains with $S > 1$ and, surprisingly, found none, although we did find cases with $\psi \neq \frac{1}{2}$ [40]. Thus, as in the other known realizations of emergent symmetries, finding a recipe for generating them poses a problem that remains wide open.

Acknowledgments— We would like to acknowledge financial support from FAPESP and CNPq.

[1] T.-P. Cheng and L.-F. Li, "Gauge Theory of Elementary Particle Physics," (Oxford, 1988) .
[2] P. W. Anderson, "Basic notions of condensed matter physics," (Benjamin-Cummings, Melon-Park, California, 1984).
[3] A. B. Zamolodchikov, Int. J. Mod. Phys. A **4**, 4235 (1989).
[4] R. Coldea, D. A. Tennant, E. M. Wheeler, E. Wawrzynska, D. Prabhakaran, M. Telling, K. Habicht, P. Smeibidl, and K. Kiefer, Science **327**, 177 (2010).
[5] K. Damle and D. A. Huse, Phys. Rev. Lett. **89**, 277203 (2002).
[6] T. Senthil, A. Vishwanath, L. Balents, S. Sachdev, and M. P. A. Fisher, Science **303**, 1490 (2004).

[7] T. Grover, D. N. Sheng, and A. Vishwanath, Science **344**, 280 (2014).
[8] H.-H. Lin, L. Balents, and M. P. A. Fisher, Phys. Rev. B **58**, 1794 (1998).
[9] C. D. Batista and G. Ortiz, Adv. Phys. **53**, 1 (2004).
[10] L. Fidkowski, H.-H. Lin, P. Titum, and G. Refael, Phys. Rev. B **79**, 155120 (2009).
[11] P. Chen, Z.-L. Xue, I. P. McCulloch, M.-C. Chung, C.-C. Huang, and S.-K. Yip, Phys. Rev. Lett. **114**, 145301 (2015).
[12] E. Zohar, J. I. Cirac, and B. Reznik, arXiv:1503.02312.
[13] J. Schmalian and C. D. Batista, Phys. Rev. B **77**, 094406 (2008).
[14] A. Imambekov, M. Lukin, and E. Demler, Phys. Rev. A **68**, 063602 (2003).
[15] J. J. García-Ripoll, M. A. Martin-Delgado, and J. I. Cirac, Phys. Rev. Lett. **93**, 250405 (2004).
[16] S. K. Ma, C. Dasgupta, and C. K. Hu, Phys. Rev. Lett. **43**, 1434 (1979).
[17] C. Dasgupta and S. K. Ma, Phys. Rev. B **22**, 1305 (1980).
[18] R. N. Bhatt and P. A. Lee, Phys. Rev. Lett. **48**, 344 (1982).
[19] F. Iglói and C. Monthus, Phys. Rep. **412**, 277 (2005).
[20] B. Boechat, A. Saguia, and M. A. Continentino, Solid State Commun. **98**, 411 (1996).
[21] R. A. Hyman and K. Yang, Phys. Rev. Lett. **78**, 1783 (1997).
[22] C. Monthus, O. Golinelli, and Th. Jolicoeur, Phys. Rev. Lett. **79**, 3254 (1997).
[23] C. Monthus, O. Golinelli, and Th. Jolicoeur, Phys. Rev. B **58**, 805 (1998).
[24] A. Saguia, B. Boechat, and M. A. Continentino, Phys. Rev. Lett. **89**, 117202 (2002).
[25] S. Bergkvist, P. Henelius, and A. Rosengren, Phys. Rev. B **66**, 134407 (2002).
[26] K. Damle, Phys. Rev. B **66**, 104425 (2002).
[27] D. S. Fisher, Phys. Rev. B **50**, 3799 (1994).
[28] S. R. Manmana, A. M. Läuchli, F. H. L. Essler, and F. Mila, Phys. Rev. B **83**, 184433 (2011).
[29] See Supplemental Material, which includes Refs. [30–35], for the relation between spin-1 SU(2) and antisymmetric SU(3) representations, additional numerical data, and discussions of the weak-disorder limit.
[30] K. Yang, R. A. Hyman, R. N. Bhatt, and S. M. Girvin, J. Appl. Phys. **79**, 5096 (1996).
[31] R. G. Pereira, (private communication).
[32] R. A. Hyman, K. Yang, R. N. Bhatt, and S. M. Girvin, Phys. Rev. Lett. **76**, 839 (1996).
[33] I. Affleck, T. Kennedy, E. H. Lieb, and H. Tasaki, Phys. Rev. Lett. **59**, 799 (1987).
[34] X. Chen, Z.-C. Gu, Z.-X. Liu, and X.-G. Wen, Science **338**, 1604 (2012).
[35] J. A. Hoyos, Phys. Rev. E **78**, 032101 (2008).
[36] K_i is a natural coupling constant when (1) is written in terms of irreducible spherical tensors, as noted in [37].
[37] K. Yang and R. N. Bhatt, Phys. Rev. Lett. **80**, 4562 (1998).
[38] J. A. Hoyos and E. Miranda, Phys. Rev. B **70**, 180401 (2004).
[39] E. Westerberg, A. Furusaki, M. Sigrist, and P. A. Lee, Phys. Rev. B **55**, 12578 (1997).
[40] V. L. Quito, J. A. Hoyos, and E. Miranda, (unpublished).
[41] In general, singlets of 6, 9,... original spins/quarks are also formed, though less abundantly [38].
[42] J. A. Hoyos, A. P. Vieira, N. Laflorencie, and E. Miranda, Phys. Rev. B **76**, 174425 (2007).

arXiv:1404.1924v2 [cond-mat.str-el] 20 Oct 2015

Supplemental Material for "Emergent SU(3) symmetry in random spin-1 chains"

V. L. Quito,[1] José A. Hoyos,[2] and E. Miranda[1]

[1] *Instituto de Física Gleb Wataghin, Unicamp, Rua Sérgio Buarque de Holanda, 777, CEP 13083-859 Campinas, SP, Brazil*
[2] *Instituto de Física de São Carlos, Universidade de São Paulo, C.P. 369, São Carlos, SP 13560-970, Brazil*

(Dated: October 22, 2015)

THE SU(3)-SYMMETRIC POINTS

We first write out in detail the 8 generators of the SU(3) group in the defining (quark) representation in terms of the spin-1 operators. The Cartesian vector and symmetric rank-2 tensor operators, S_μ and $T_{\mu\nu} = S_\mu S_\nu + S_\nu S_\mu$ $(\mu, \nu = x, y, z)$, form a complete basis set of 9 elements spanning the space of 3×3 Hermitian matrices. The generators we seek are the complete set of 8 *traceless* Hermitian matrices. A convenient choice is

$$\Lambda_1 = S_x, \tag{1}$$
$$\Lambda_2 = S_y, \tag{2}$$
$$\Lambda_3 = S_z, \tag{3}$$
$$\Lambda_4 = S_x S_y + S_y S_x, \tag{4}$$
$$\Lambda_5 = S_x S_z + S_z S_x, \tag{5}$$
$$\Lambda_6 = S_y S_z + S_z S_y, \tag{6}$$
$$\Lambda_7 = S_x^2 - S_y^2, \tag{7}$$
$$\Lambda_8 = \frac{1}{\sqrt{3}}\left(2S_z^2 - S_x^2 - S_y^2\right). \tag{8}$$

In terms of these generators, the linear Heisenberg term is obvious, whereas the bilinear term can be written as

$$\left(\mathbf{S}\cdot\mathbf{S}'\right)^2 = \frac{4}{3} - \frac{1}{2}\sum_{a=1}^{3}\Lambda_a\Lambda'_a + \frac{1}{2}\sum_{a=4}^{8}\Lambda_a\Lambda'_a. \tag{9}$$

The generic Hamiltonian for two adjacent sites in terms of θ $(\tan\theta = D/J)$ is

$$H(\theta) = \cos\theta\,\mathbf{S}\cdot\mathbf{S}' + \sin\theta\left(\mathbf{S}\cdot\mathbf{S}'\right)^2 \tag{10}$$
$$= \frac{4}{3}\sin\theta + \left(\cos\theta - \frac{1}{2}\sin\theta\right)\sum_{a=1}^{3}\Lambda_a\Lambda'_a \tag{11}$$
$$+\frac{1}{2}\sin\theta\sum_{a=4}^{8}\Lambda_a\Lambda'_a. \tag{12}$$

The point $\theta = \frac{\pi}{4}$ then becomes

$$H\left(\theta = \frac{\pi}{4}\right) \propto \mathbf{S}\cdot\mathbf{S}' + \left(\mathbf{S}\cdot\mathbf{S}'\right)^2 \tag{13}$$
$$= \frac{4}{3} + \frac{1}{2}\sum_{a=1}^{8}\Lambda_a\Lambda'_a, \tag{14}$$

whose SU(3) invariance is manifest. The other SU(3)-invariant point at $\theta = -\frac{\pi}{2}$ is

$$H\left(\theta = -\frac{\pi}{2}\right) = -\left(\mathbf{S}\cdot\mathbf{S}'\right)^2 \tag{15}$$
$$= -\frac{4}{3} + \frac{1}{2}\sum_{a=1}^{3}\Lambda_a\Lambda'_a - \frac{1}{2}\sum_{a=4}^{8}\Lambda_a\Lambda'_a. \tag{16}$$

In order to make the SU(3) invariance manifest in this case, we must first realize that the antiquark representation, the complex conjugate of the quark one, is obtained by applying the following operation to the generator matrices

$$\left(\Lambda_a\right)_{ij} \to -\left(\Lambda_a\right)^*_{ij}. \tag{17}$$

We get (assuming the usual basis of eigenvectors of S_z)

$$\Lambda_1 \to -S_x, \tag{18}$$
$$\Lambda_2 \to S_y, \tag{19}$$
$$\Lambda_3 \to -S_z, \tag{20}$$
$$\Lambda_4 \to S_x S_y + S_y S_x, \tag{21}$$
$$\Lambda_5 \to -S_x S_z - S_z S_x, \tag{22}$$
$$\Lambda_6 \to S_y S_z + S_z S_y, \tag{23}$$
$$\Lambda_7 \to -S_x^2 + S_y^2, \tag{24}$$
$$\Lambda_8 \to -\frac{1}{\sqrt{3}}\left(2S_z^2 - S_x^2 - S_y^2\right). \tag{25}$$

An equivalent representation to Eqs. (18)-(25) is obtained if we make a rotation of π around the y-axis: $S_x \to -S_x$, $S_z \to -S_z$. After these transformations, we find, denoting the antiquark representation by a tilde,

$$\tilde{\Lambda}_a = \Lambda_a \ (a = 1, 2, 3), \tag{26}$$
$$\tilde{\Lambda}_a = -\Lambda_a \ (a = 4, 5, 6, 7, 8). \tag{27}$$

From Eqs. (16) and (26)-(27), we see that the $\theta = -\frac{\pi}{2}$ point couples sites belonging to the quark and the antiquark representations

$$H\left(\theta = -\frac{\pi}{2}\right) = -\frac{4}{3} + \frac{1}{2}\sum_{a=1}^{8}\Lambda_a\tilde{\Lambda}'_a. \tag{28}$$

Note that the FM points $\theta = -\frac{3\pi}{4}$ and $\theta = \frac{\pi}{2}$ also display global SU(3) invariance since

$$H\left(\theta = \frac{\pi}{2}\right) = -H\left(\theta = -\frac{\pi}{2}\right), \tag{29}$$
$$H\left(\theta = \frac{3\pi}{4}\right) = -H\left(\theta = \frac{\pi}{4}\right). \tag{30}$$

NUMERICAL RESULTS

We have implemented the full SDRG procedure described in the main text numerically in order to check our findings. We have first focused on initial Hamiltonians in which all bonds have the same $\theta_i = \theta_0$ with $-\frac{3\pi}{4} < \theta_0 < \frac{\pi}{2}$, while J is uniformly distributed in the interval $0 \leq J \leq 1$. The results were obtained for chain lengths of $L_0 \sim 10^6$ spins, averaged over 20 realizations of disorder. We have verified that, although initially the θ distribution broadens, *asymptotically all θ_i tend to unique values*.

In Fig. 1, we show, for some representative cases, the average value of $\tan\theta$ as the mean distance L between undecimated spin clusters is increased. The latter is given by $L = \frac{L_0}{N}$, where N is the number of undecimated spin clusters. For $-\frac{\pi}{2} < \theta_0 < \frac{\pi}{4}$ (three blue lowest curves), the flow is towards the FP (1), with $\theta = 0$. When $-\frac{3\pi}{4} < \theta_0 < -\frac{\pi}{2}$ (red, topmost curve), the flow tends to the FP (2), with $\tan\theta = 2$, $D < 0$. The green (2nd and 3rd from the top) curves correspond to the interval $\frac{\pi}{4} < \theta_0 < \frac{\pi}{2}$, for which the systems flows to the FP (3), $\tan\theta = 2$, $D \lessgtr 0$ with equal probability. For the specific case of $\theta_0 = \frac{\pi}{4}$ (black curve with down triangles), we plotted instead the inverse of $\langle\cot\theta\rangle$ on the right-hand vertical axis. This corresponds to flows at the unstable FP (8), for which asymptotically half the bonds have $\theta = -\frac{\pi}{2}$ and half $\theta = \frac{\pi}{4}$, such that $\langle\cot\theta\rangle \to 1/2$. These plots confirm the delineation of the fixed points and basins of attraction described in the main text.

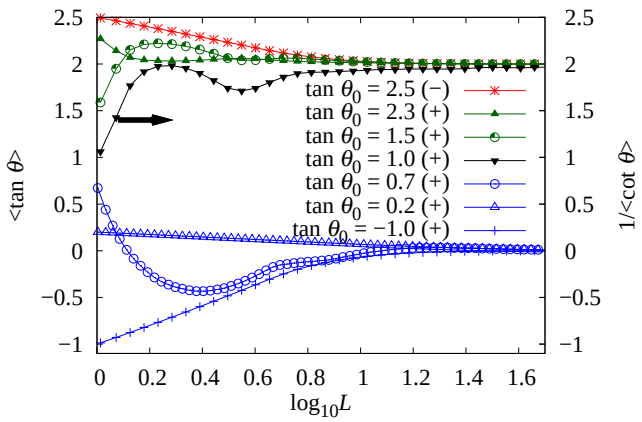

Figure 1. (Color online) Some representative SDRG flows: mean value of $\langle\tan\theta\rangle$ as a function of the average distance L between undecimated spin clusters, for different values of the angle θ_0 of the initial distribution. The sign in parentheses is the sign of J's in the initial distribution. For $\tan\theta_0 = 1$, we plot $\frac{1}{\langle\cot\theta\rangle}$ on the right-hand vertical axis instead.

Although the flow in the region $(-\frac{\pi}{2} < \theta_0 < \frac{\pi}{4})$ is characterized by the disappearance of the biquadratic couplings, there is a clear difference in the transient SDRG flow between the cases $\arctan\frac{1}{3} < \theta_0 < \frac{\pi}{4}$ and $-\frac{\pi}{2} < \theta_0 < \arctan\frac{1}{3}$. The latter only involves singlet-forming decimations [see Eq. (2) and Fig. 2 of the main text]. As a result, $\langle\tan\theta\rangle$ flows monotonically to 0 ($\tan\theta_0 = 0.2$ and -1 in Fig. 1). When $\arctan\frac{1}{3} < \theta_0 < \frac{\pi}{4}$, however, both types of decimations rules occur [Eqs. (2) and (3) of the main text], necessarily generating negative angles, in such a way that $\langle\tan\theta\rangle$ may change sign in the course of the flow ($\tan\theta_0 = 0.7$ in Fig. 1).

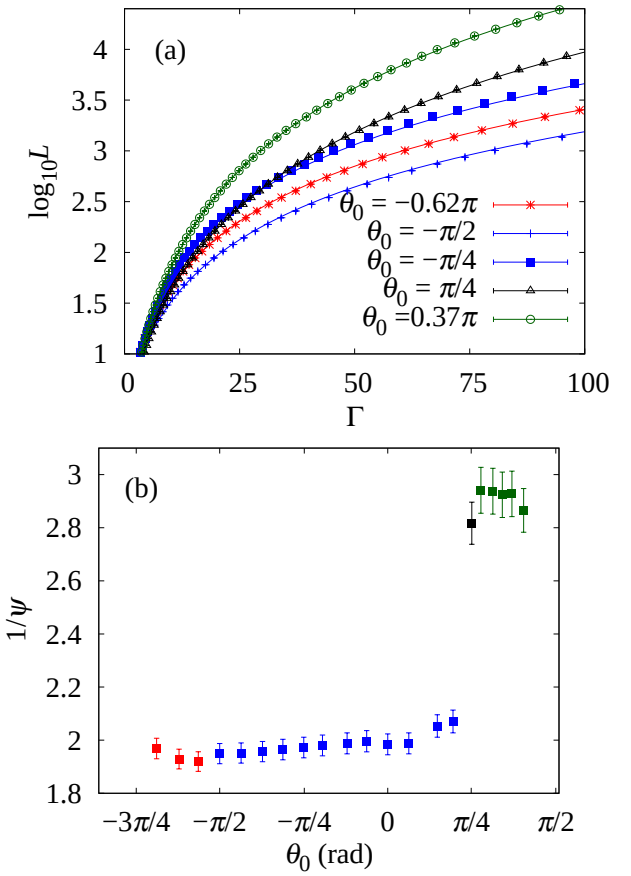

Figure 2. (Color online) Numerical determination of the ψ exponent: (a) mean distance L between undecimated spin clusters as a function of $\Gamma = \ln\frac{\Omega_0}{\Omega}$, where Ω is the renormalization group energy scale. The full lines are fits to Eq. (31); (b) reciprocal of the activated dynamical scaling exponent ψ as a function of initial angle θ_0.

In order to numerically determine the value of ψ in each of the RSPs of the phase diagram, we tracked the dependence of the cutoff energy scale $\Gamma \equiv \ln\frac{\Omega_0}{\Omega}$ (where Ω_0 is the largest initial Δ_i) on the average distance between undecimated spin clusters L. In Fig. 2(a) we show the results for several initial angles θ_0. We have fitted our data to the form

$$\log_{10} L = a + \frac{1}{\psi}\log_{10}(1 + b\Gamma)\,, \qquad (31)$$

where a, b and $\frac{1}{\psi}$ are fitting parameters. As seen in Fig. 2(a), it fits remarkably well the numerical data. For $b\Gamma \gg 1$, we recover the more familiar activated dynamical scaling form $L \sim \Gamma^{\frac{1}{\psi}}$. The numerically determined values of ψ can be seen in Fig. 2(b) as a function of θ_0. There is good agreement with the predicted exponents of the mesonic ($\psi_M = \frac{1}{2}$) and baryonic ($\psi_B = \frac{1}{3}$) RSPs and a sharp jump at the border between them ($\theta_0 = \frac{\pi}{4}$) can be clearly seen. The error bars were estimated from the uncertainty in the range over which Eq. 31 is valid.

BEHAVIOR AT WEAK DISORDER

The spontaneously dimerized phase ($-\frac{3\pi}{4} < \theta < -\frac{\pi}{4}$) is unstable against weak disorder due to the formation of weakly coupled domain walls [1, 2]. Weak disorder can also be shown to be a relevant perturbation at the SU(3)-symmetric point $\theta = \frac{\pi}{4}$ [3]. In general, we expect disorder to be perturbatively relevant in the entire gapless phase $\frac{\pi}{4} \leq \theta \leq \frac{\pi}{2}$.

Infinitesimally weak disorder is an irrelevant perturbation in the gapped Haldane phase ($-\frac{\pi}{4} < \theta < \frac{\pi}{4}$). The behavior was determined in detail at $\theta_i = 0$ [2, 4–7]. Gradually increasing the disorder at this point eventually leads to the closure of the Haldane gap (although the topological order parameter initially retains a finite value [8]) and to the emergence of a quantum Griffiths region [9] with conventional power-law scaling $\Omega \sim L^{-z}$. In this region, the spin correlations are short ranged, the magnetic susceptibility $\chi \sim T^{1/z-1}$, and the specific heat $c \sim T^{1/z}$. The dynamical exponent z is disorder-dependent and diverges at a critical point [4–7, 9, 10]. Above this critical disorder value, the system enters a universal RSP governed by an IRFP with $\psi = \frac{1}{2}$. This generic behavior is expected to hold throughout the region $-\frac{\pi}{4} < \theta < \frac{\pi}{4}$, with the exception of the AKLT point.

At the AKLT point ($\theta = \arctan\frac{1}{3}$), the ground state is exactly known [11]. Provided the local angle θ_i is everywhere equal to $\arctan\frac{1}{3}$, the ground state will be disorder independent [12]. We note that this is reflected in the SDRG procedure by the closure of the gap of a spin pair $\Delta_i = 3J_i\left|\tan\theta_i - \frac{1}{3}\right|$, which makes it ill-defined in the vicinity of the AKLT point. The Haldane gap, however, will vanish in the strong-disorder limit when the distribution of coupling constants is not bounded from below.

Although tailored to be accurate only in the strong disorder regime, the SDRG flow has been shown to break down whenever weak disorder is irrelevant [2, 4–7, 9, 13]. This is signaled by the fact that the coupling constant distributions do not broaden as the energy scale is reduced. We only detect this break-down in the topological phase $-\frac{\pi}{4} < \theta < \frac{\pi}{4}$ [14]. In fact, our numerics indicate that weak disorder may possibly be relevant even inside the Haldane phase near the edges $\pm\frac{\pi}{4}$. Since the dimerized ($-\frac{3\pi}{4} < \theta < -\frac{\pi}{4}$) and the gapless ($\frac{\pi}{4} < \theta < \frac{\pi}{2}$) phases are expected to be destabilized by any amount of disorder and we have not found any other fixed point numerically, we conjecture that no other phase transition happens at intermediate disorder strength. We thus obtain the weak disorder region of the phase diagram sketched in Fig. 1 of the main text.

[1] K. Yang, R. A. Hyman, R. N. Bhatt, and S. M. Girvin, J. Appl. Phys. **79**, 5096 (1996).
[2] B. Boechat, A. Saguia, and M. A. Continentino, Solid State Commun. **98**, 411 (1996).
[3] R. G. Pereira, Private communication.
[4] R. A. Hyman and K. Yang, Phys. Rev. Lett. **78**, 1783 (1997).
[5] C. Monthus, O. Golinelli, and T. Jolicoeur, Phys. Rev. Lett. **79**, 3254 (1997).
[6] C. Monthus, O. Golinelli, and Th. Jolicoeur, Phys. Rev. B **58**, 805 (1998).
[7] A. Saguia, B. Boechat, and M. A. Continentino, Phys. Rev. Lett. **89**, 117202 (2002).
[8] R. A. Hyman, K. Yang, R. N. Bhatt, and S. M. Girvin, Phys. Rev. Lett. **76**, 839 (1996).
[9] K. Damle, Phys. Rev. B **66**, 104425 (2002).
[10] S. Bergkvist, P. Henelius, and A. Rosengren, Phys. Rev. B **66**, 134407 (2002).
[11] I. Affleck, T. Kennedy, E. H. Lieb, and H. Tasaki, Phys. Rev. Lett. **59**, 799 (1987).
[12] X. Chen, Z.-C. Gu, Z.-X. Liu, and X.-G. Wen, Science **338**, 6114 (2012).
[13] J. A. Hoyos, Phys. Rev. E **78**, 032101 (2008).
[14] In this case, it is still possible to use the SDRG through an appropriate generalization of the recursion relations as in reference [5].